Science Advances
AAAS

Supplementary Materials for

Reconstruction of distinct vertebrate gastrulation modes via modulation of key cell behaviors in the chick embryo

Manli Chuai *et al.*

Corresponding author: Guillermo Serrano Nájera, gs714@cam.ac.uk; Cornelis J. Weijer, c.j.weijer@dundee.ac.uk

Sci. Adv. **9**, eabn5429 (2023)
DOI: 10.1126/sciadv.abn5429

The PDF file includes:

Other Supplementary Material for this manuscript includes the following:

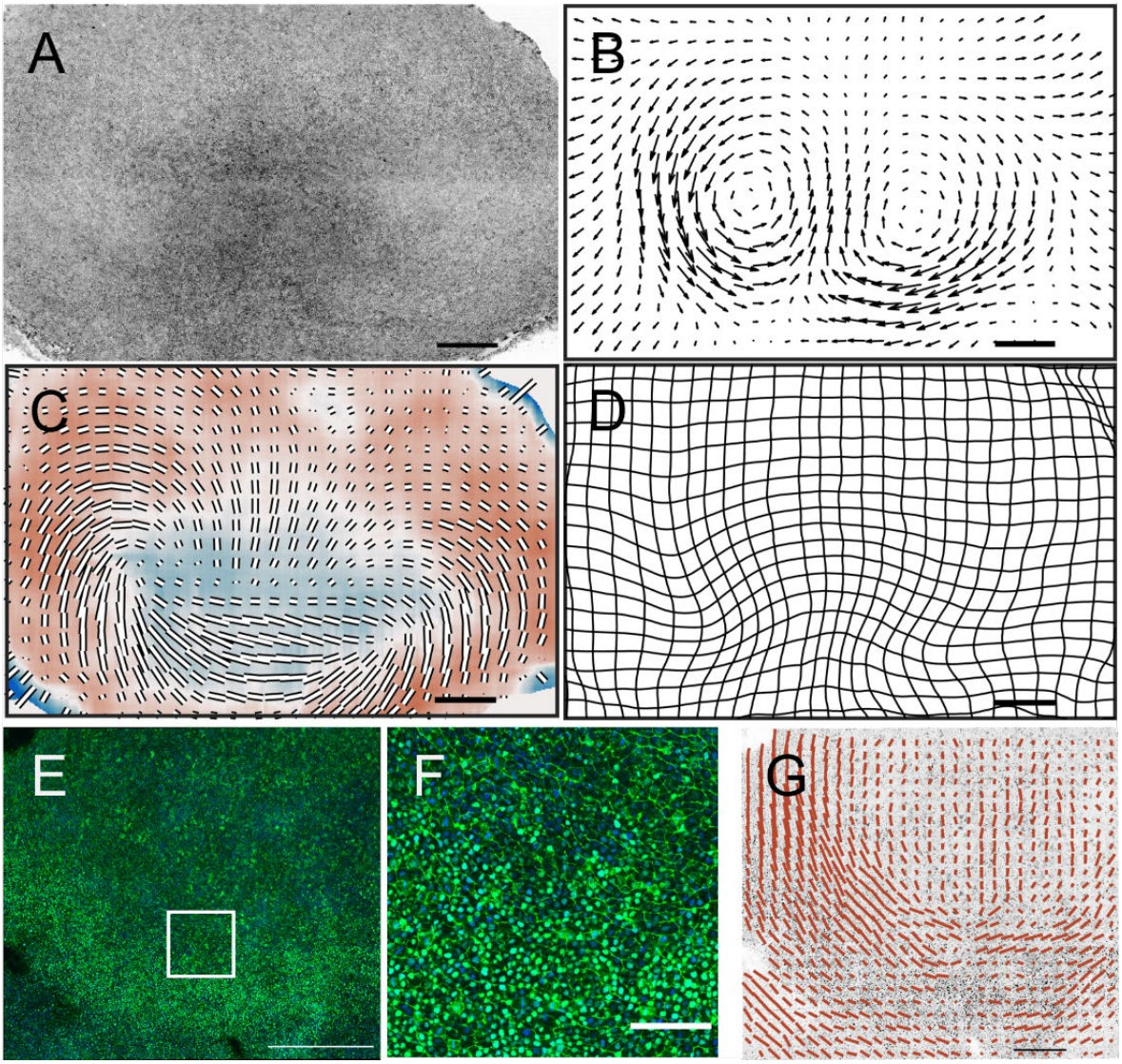

Fig. S1. Correlation of tissue flow, deformation speed, cell shape, and myosin distribution and alignment. **(A**) Epiblast view of HH2 stage embryo in light sheet microscope (**B**) Velocity field for the embryo (HH2) shown in A. (**C**) Strain rate tensor, isotropic component color coded red-blue, the anisotropic component is shown as black bars in direction of contraction. (**D**) Deformation grid calculated from stage HH1 to current stage HH2 for embryo shown in A. D: SNAI and phosphor-myosin light chain in HH2 stage embryo. (**E**) Overview image of pMLC and SNAI2 straining in the posterior region of an HH2 embryo. (**F**) High magnification image of section in the white box shown in E showing myosin cables and nuclear SNAI staining. **(G)** Myosin anisotropy computed for embryo shown in E. Scale bars in A-F 500 μm. In C the scale bar length represents ~ 0.5 1/h for the anisotropic component of the strain rate. In G the scale bar represents 250 μm and ~ 70% anisotropy.

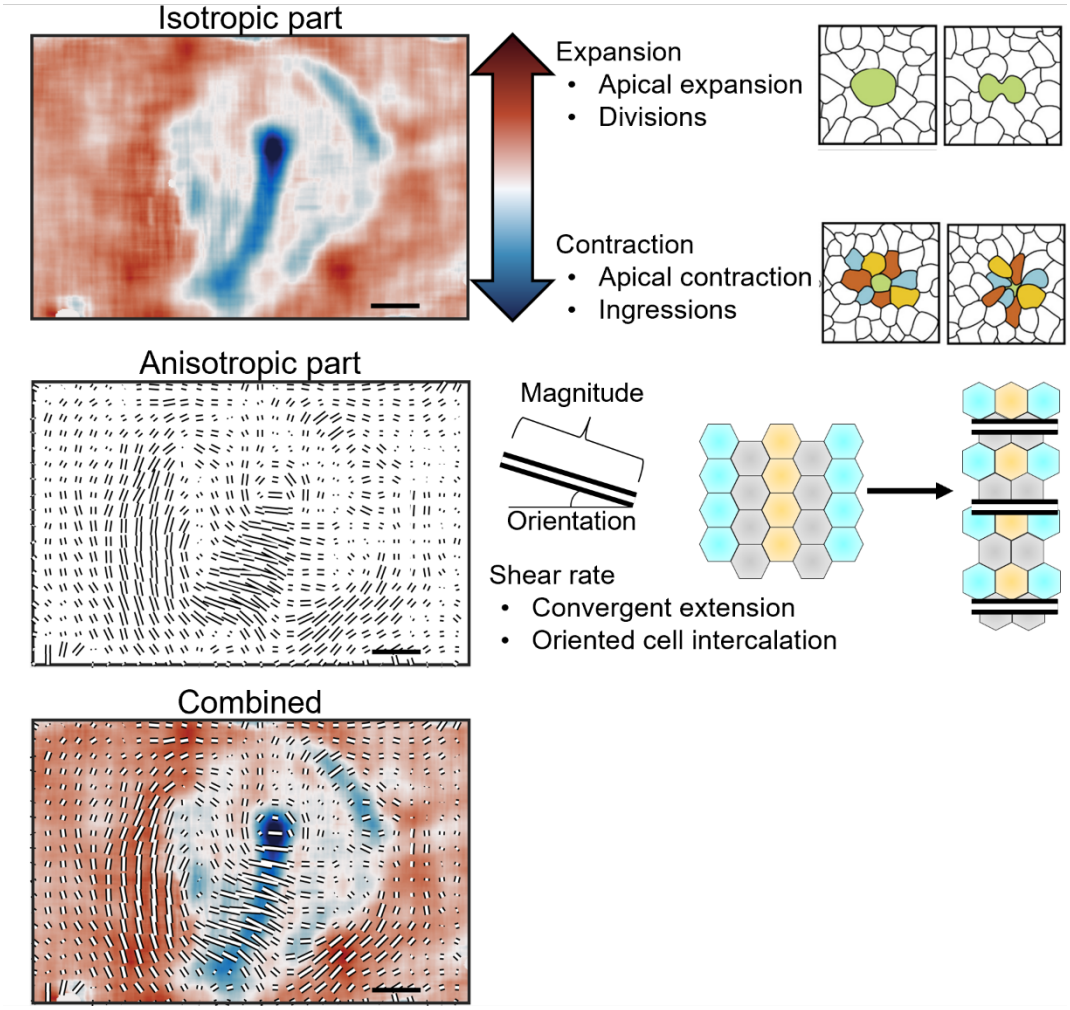

Fig. S2. The decomposed strain rate tensor indicates the cell behaviors underlying the tissue flows on a continuous epithelial layer. Top, The Isotropic part of the strain rate describes how the tissue is changing in the area. Positive values (red) indicate tissue expansion, produced by a combination of apical expansion and cell proliferation. Negative values (blue) indicate contraction, produced by apical contraction and cell ingressions. Middle: The anisotropic part of the strain rate tensor represents the rate of pure shear deformation. The orientation of the bars indicates that the tissue is contracting along the bar while expanding in the perpendicular direction without changing the area. The length of the bar represents the magnitude of the shear deformation rate. In the chick embryo, most of the shear rate is explained by oriented cell intercalations (15). Bottom: The combination of the isotropic and anisotropic components of the strain rate provides a clear indication of the key cell behaviors underlying the tissue flows.

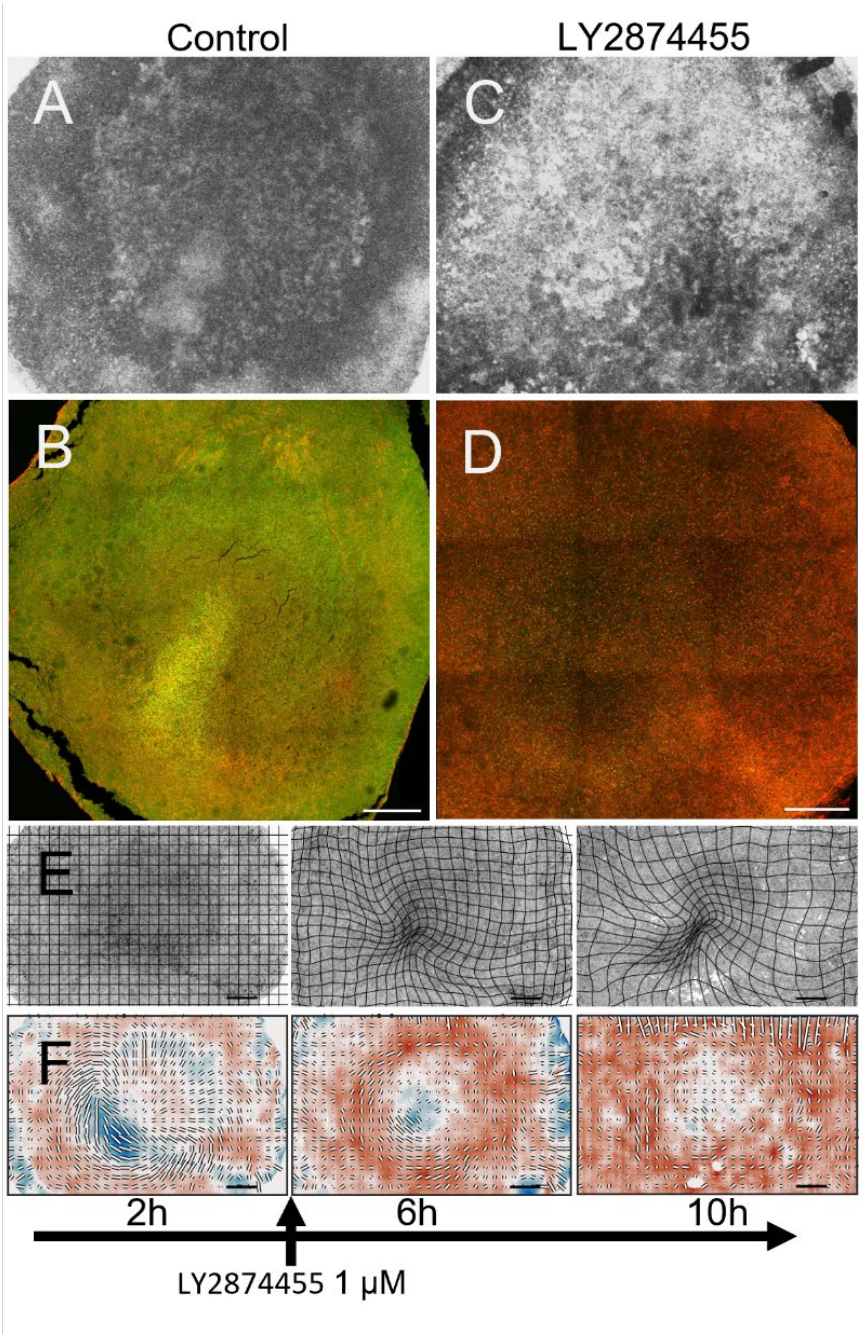

Fig. S3. Inhibition of FGF signaling blocks mesoderm differentiation and streak formation. (**A)**, surface view of control embryo after 16hrs of development in EC culture. (**B**), Composite confocal imager of SNAI (green) and actin (red) of the embryo is shown in A. (**C**), Embryo after 16hrs of treatment with the FGF receptor inhibitor LY2874455 (1uM). (**D**), Composite confocal imager of SNAI (green) and actin (red) of the embryo shown in C, showing absence of SNAI expression. (**E)**, Three successive times of embryo images in light sheet 4, 8, and 12 hours faster addition of LY2874455 (1uM). Note that LY2874455 treated embryos fail in generating a primitive streak (3/3 in the light sheet microscope). (**F**), strain rate tensor at 4,8 and 12 hours for embryo shown in C. Scale bars for E and F as in Fig. S1 C.

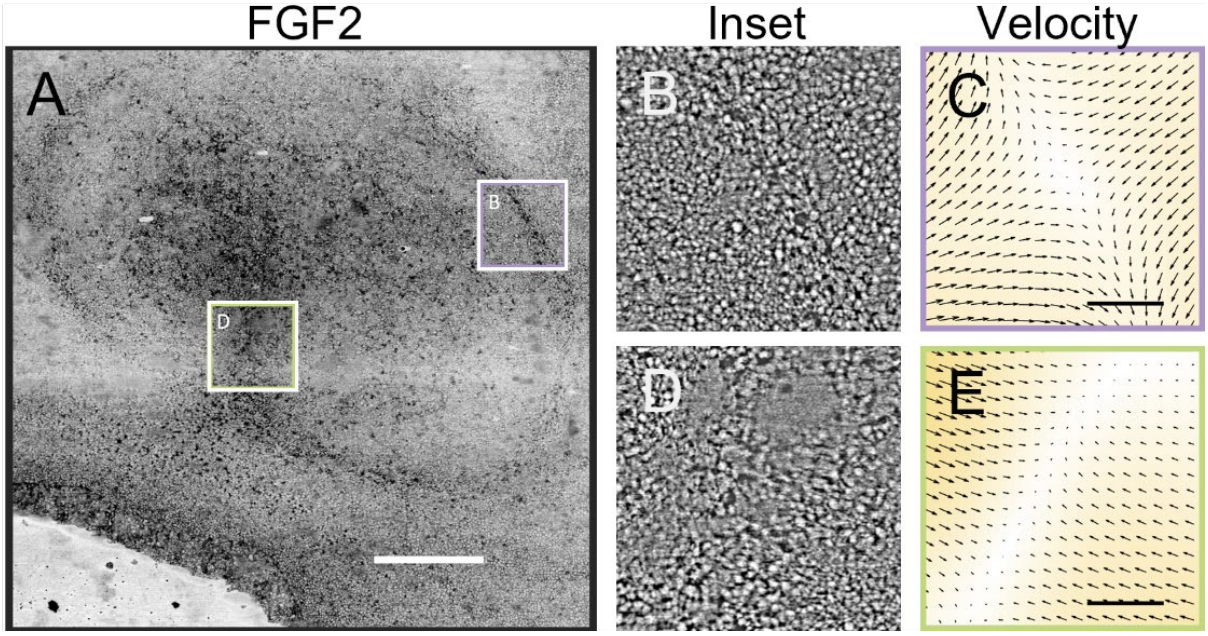

Fig. S4. **Convergent extension on the circular primitive streak generated by FGF2 addition.** (**A**), Overview images of embryo treated with FGF (50 µg/mL) from light sheet microscope after 13h. (**B**), Close up of the circular primitive streak generated by FGF addition (see Movie S4). (**C**), Velocity field calculated on B shows convergence extension flows along the circular primitive streak. (**D**), Close-up of the original primitive streak. (**E**), Velocity field calculated on D showing convergence extension flows along the original primitive streak.

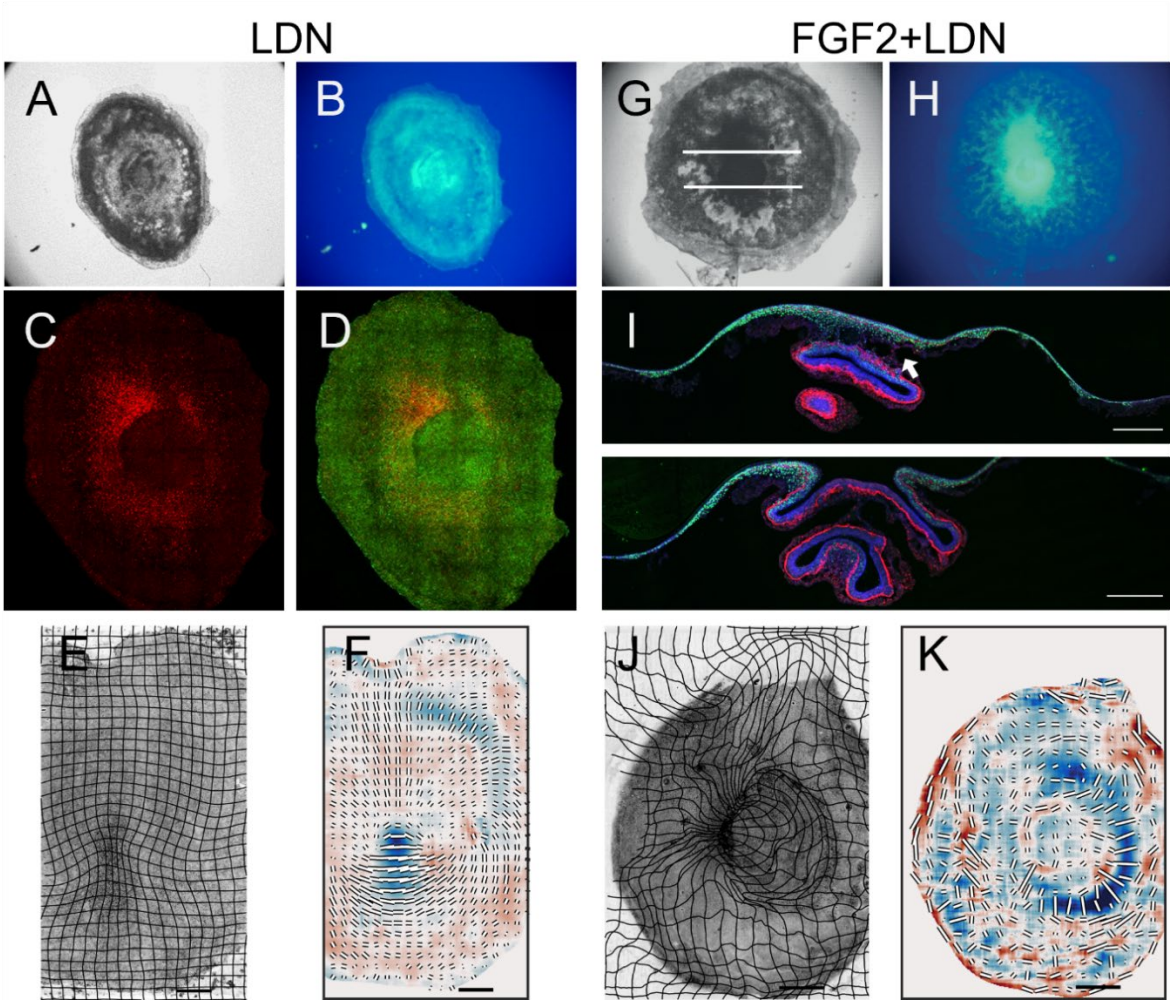

Fig. S5 Changes in gastrulation morphology after interfering with BMP and FGF signaling. (A), widefield image of embryo treated for 16hrs with LDN-193189 for 16hrs. (**B**), Widefield image of (S19)phospho-myosin light chain expression of the embryo shown in A. (**C**), Confocal image of SNAI expression of the embryo shown in A. (**D**), Confocal image of (S19) phospho-myosin light chain and SNAI expression in embryo shown in A. (**E**), light sheet microscopy images of an embryo treated with LDN-193189 (100nM) for 10 hours. (**F**), Strain rate tensor for embryo shown in E. Typically, LDN-193189 treated embryos (100nM) generate a large depression at the boundary between the epiblast, and the consequent invagination of the central epiblast, that results in the detachment of the embryo from the vitelline membrane when cultured in the light-sheet microscope (5/5 embryos in the light sheet microscope). (**G**), Widefield image of an embryo after treatment of LDN-193189 and FGF2 for 16hrs. (**H**), Widefield image of (S19)phospho-myosin light chain expression of the embryo shown in G. (**I**), Two sections through embryo shown in G at the position of white lines. (**J**), Lightsheet microscopy images of embryo treated with LDN-193189 (100nM) and FGF2 (50 µg/mL) for 15 hours. (**K**), Strain rate tensor for embryo shown in J. In LDN-193189 + FGF2 the LDN-193189 phenotype dominates at the morphogenetic level, generating a large invagination that engulfs the epiblast (6/7 embryos in the lightsheet microscope). Scale bars as in figure 1, except in I where the scale bars are 250 μm. Scale bar for K as in Fig. S1 C.

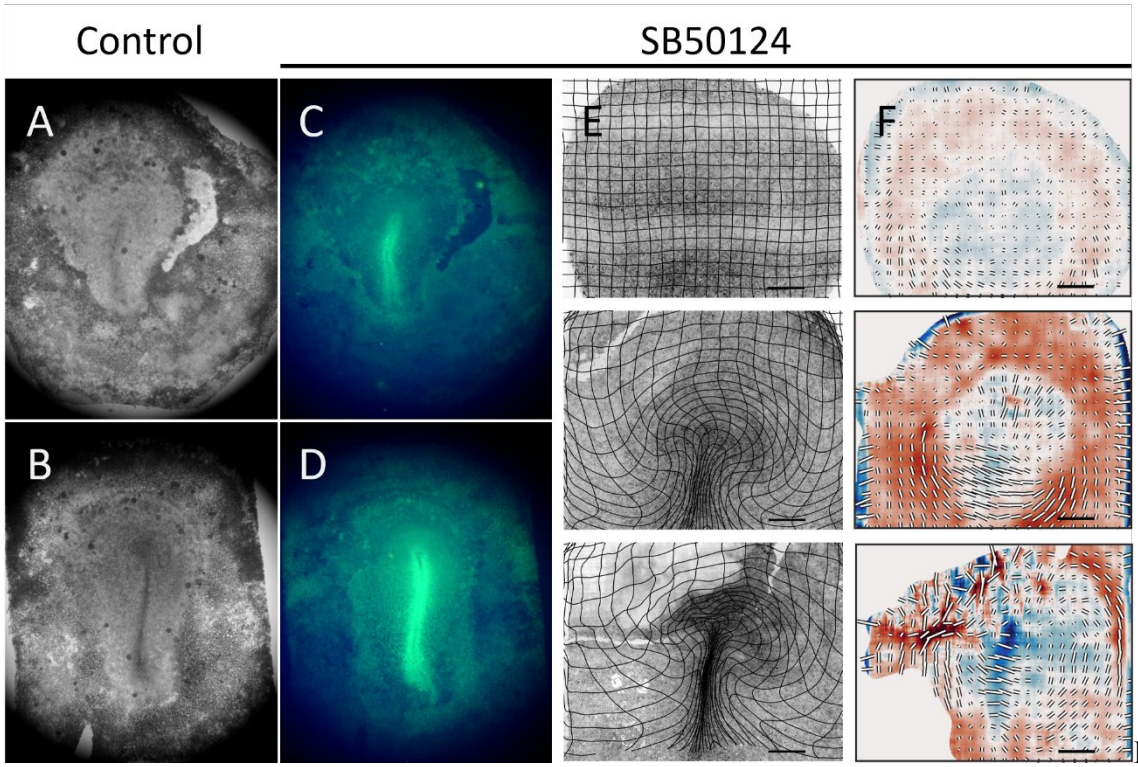

Fig. S6 Inhibition of Nodal signaling partly inhibits streak formation. (**A**), widefield image of control embryo after 16hrs development in EC culture**. (B**), Embryo after 16hrs incubation in EC culture with the Nodal signaling inhibitor SB50124 (10 μM). (**C**), SNAI expression in embryo shown in A. (**D**), SNAI expression in embryo shown in A. (**E**), Surface view of embryo in light sheet microscope 2, 4, and 8 hours (from top to bottom) the after addition of SB50124 (10 μM). (**F**), Strain rate tensor of the embryo at successive times shown in E (2/2 in the light sheet microscope). Scale bars 500 μm. Scale bars for F as in Fig. S1 C.

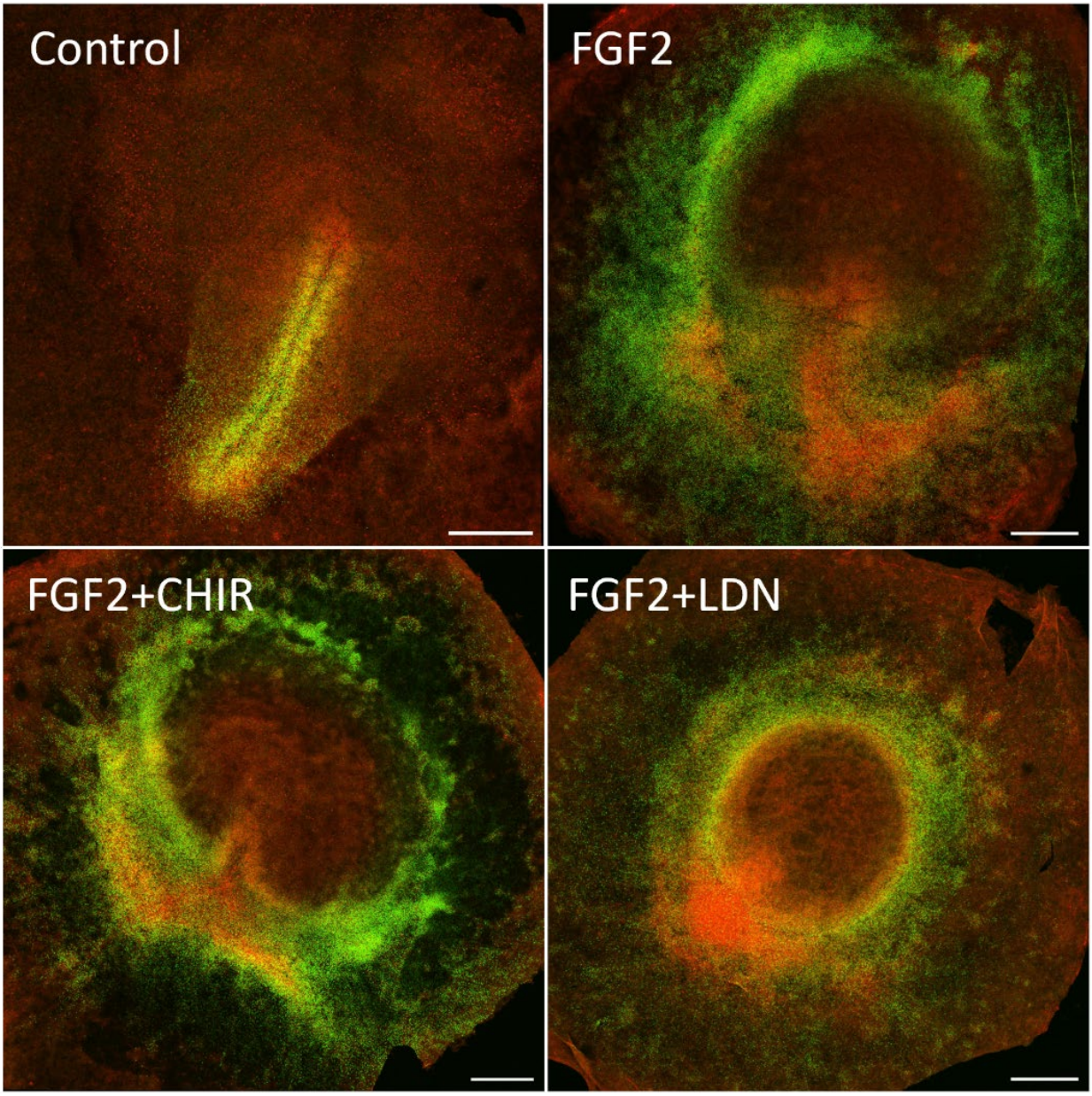

Fig. S7 Effect of perturbation of different signaling pathways on mesoderm formation and Localisation. Merged images showing SNAI2 expression (green) and actin (red) localization after 16hrs of varying treatments as indicated in legends. Control experiments show that the very tip of the streak is devoid of SNAI2 expression. FGF treatment results in a ring of mesoderm expression at the embryonic extraembryonic interface. Combined FGF and CHIR treatment results in very similar phenotypes as FGF alone. FGF treatment combined with inhibition of BMP signaling reinforces mesoderm differentiation in the ring and results in tissue buckling and suppresses streak formation and extension. Scale bars 500µm.

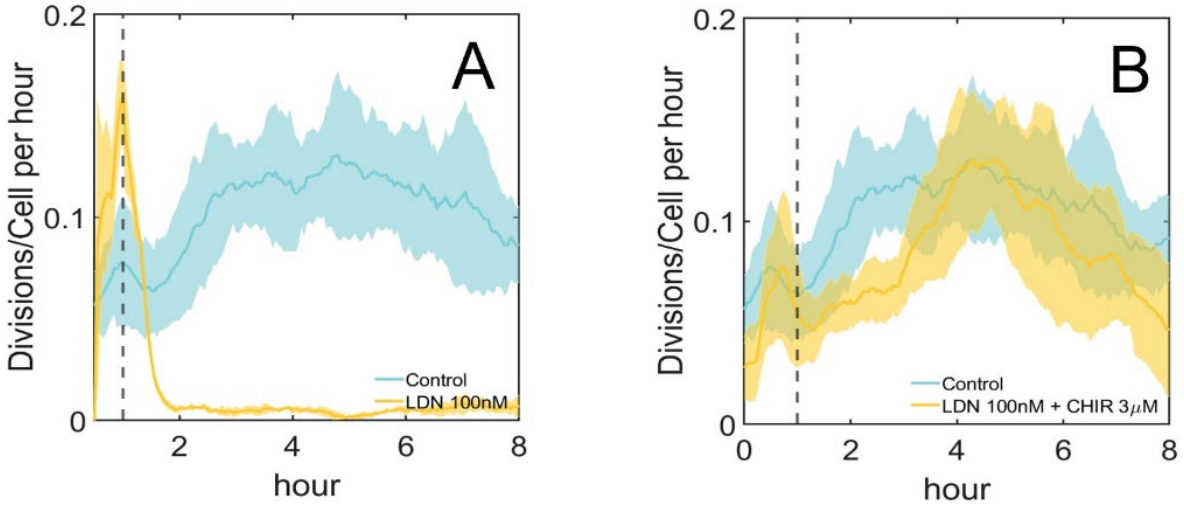

Fig. S8. CHIR rescues cell division in LDN-193189 treated embryos. (A), Cell division rate in embryos during LDN-193189 (100 nM) compared to control (not treated). (**B**), Cell division rate in embryos during LDN-193189 (100 nM) + CHIR (3 μM) compared to control (not treated). All curves show means and standard errors of division rates in at least 3 embryos

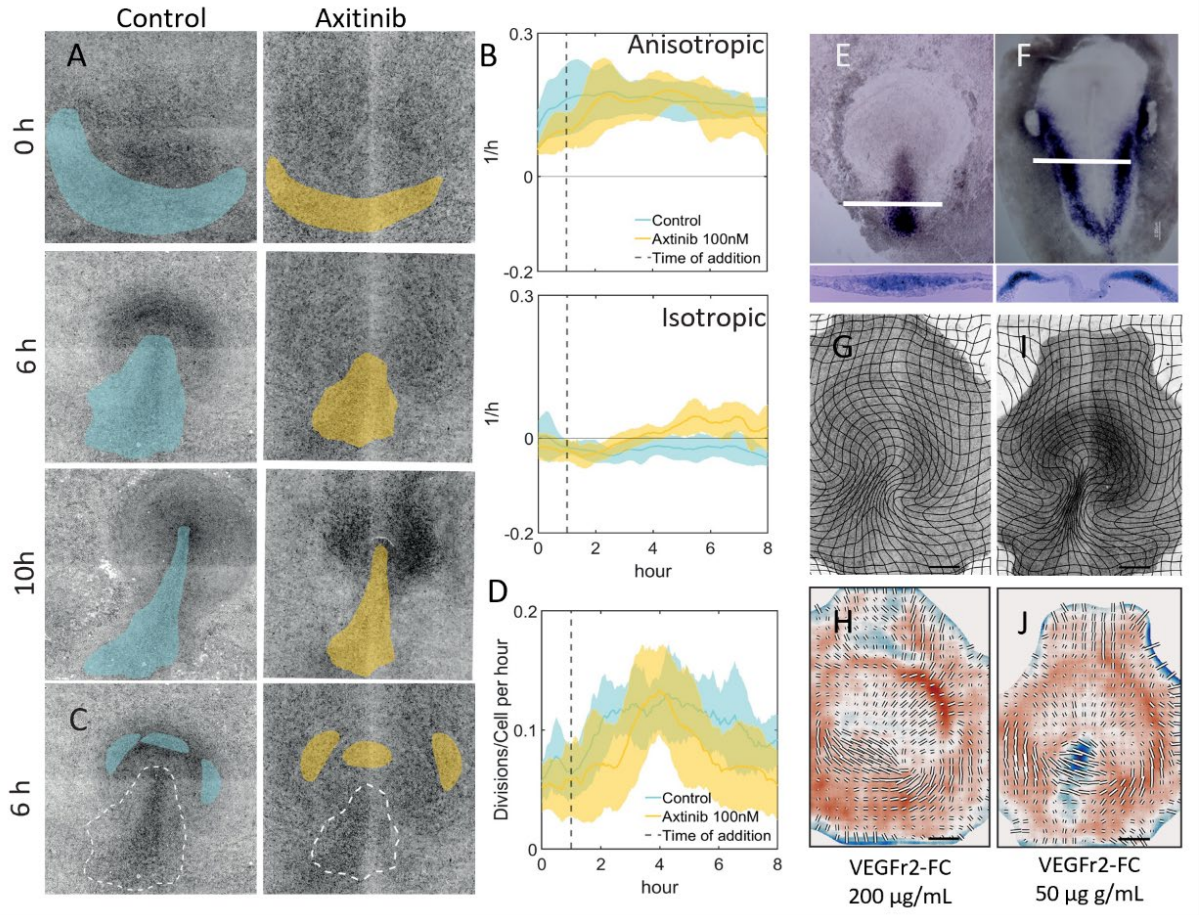

Fig. S9 Inhibition of VEGF signaling results in loss of ingression but does not inhibit intercalation. (A), Comparison of control embryo Left column and an embryo treated with the VEGF signaling inhibitor Axitinib (100nM) (right column). Images are overlaid with areas that correspond to the mesendoderm territories as determined from the dynamic morphoskeleton for the control embryo (blue) and axitinib embryo (yellow). (**B**), Strain rate tensor quantified in the blue and yellow areas in A, showing that in the control case the isotropic strain rate (upper panel) becomes negative, while in the axitinib treated embryos the isotropic component stays positive showing a lack of contraction, while the anisotropic strain component is high in both cases showing significant intercalation. The curves shown represent the mean and standard error of four or more embryos in each case. (**C, D**), Analysis of cell division rate in selected areas of the anterior epiblast of control and axitinib treated embryos. For each embryo, three analysis regions anterior to the streak (C) were followed over time and the rate of cell division (D) was calculated. The results show that axitinib treatment does not affect the rate of cell divisions. The curves in D are the average and standard errors of three regions for three embryos for each treatment. (**E, F**), In situ hybridization of the VegfR2 receptor at two stages of development (HH3 and HH5), sections show that the receptor is expressed in mesendoderm before and after ingression. (**G**): Epiblast view and deformation grid of embryo treated for 16hrs with VegfR2 Fc fragments to deplete its ligands in the light sheet microscope. (**H**), Strain rate tensor for embryo shown in H. Note the presence of intercalation of a strong anisotropic component (black bars) showing intercalation, but an absence of a negative isotropic component (blue), showing a lack of

ingression (2/2 embryos treated with VEGFr2-FC 50 µg/mL and 3/3 embryos treated with VEGFr2-FC 200 µg/mL in the light sheet microscope). (**I, J**), Lower VegfR2-Fc concentrations show a partial inhibition of streak formation. Scale bars for H, J as in Fig. S1 C.

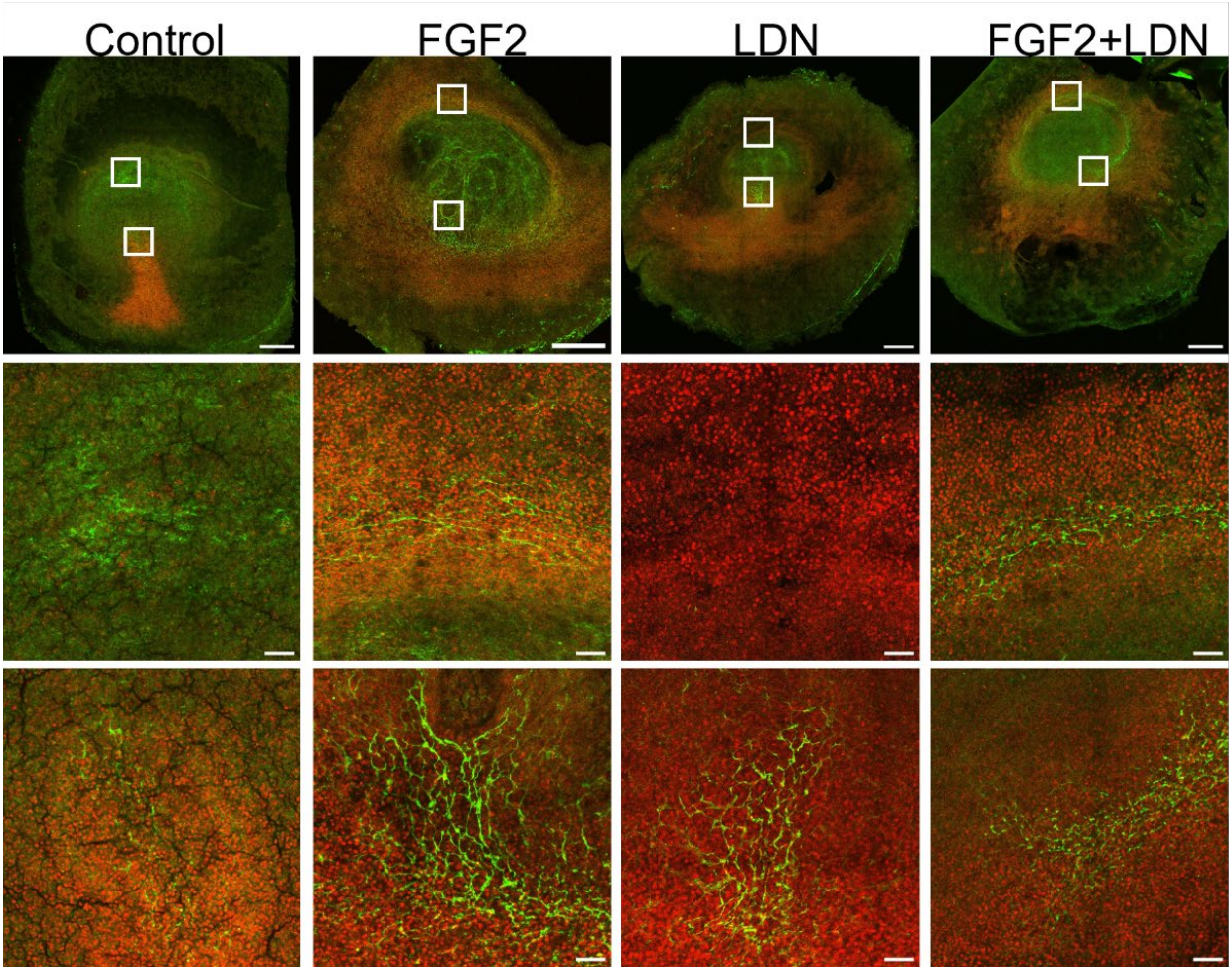

Fig. S10 Comparison of SNAI2 and TNC expression after various perturbations. Top row: Brightfield images of embryos after 16hrs in EC culture after various treatments. Second row: Confocal images of the embryos in the top row showing expression of SNAI2 (red) and TNC (green). The third and fourth rows show higher magnification images taken in front of the streak (upper white square in each image) and (lower white square in each image) at the tip of the streak. It can be seen in the control (first row) that the region anterior to the streak expresses high levels of TNC which forms a meshwork of fibrils elongated in the direction of the streak. TNC expression can also be detected in front of the streak, but it is present as a random meshwork of finer fibrils. After FGF treatment (second column) TNC expression shows the same large elongated fibrillar structure as seen in the streak of control embryos, indicating that this is also a region where cells ingress and EMT is taking place. LDN treatment TNC shows an elongated fibrillar structure in the remnant of the streak, but the anterior region shows only very low levels of TNC expression and the absence of any fibrillar network, indicating that little ingression and EMT is taking place in this region. Interestingly a combination treatment of LDN and FGF results in a clear fibrillar network indicating that EMT is taking pace and ingression will occur. The data show that the presence or absence of ingression is reflected in the FN1 network structure. Scale bars in two top rows of images are 500 μm, and scale bars in two bottom rows of images are 50 μm.

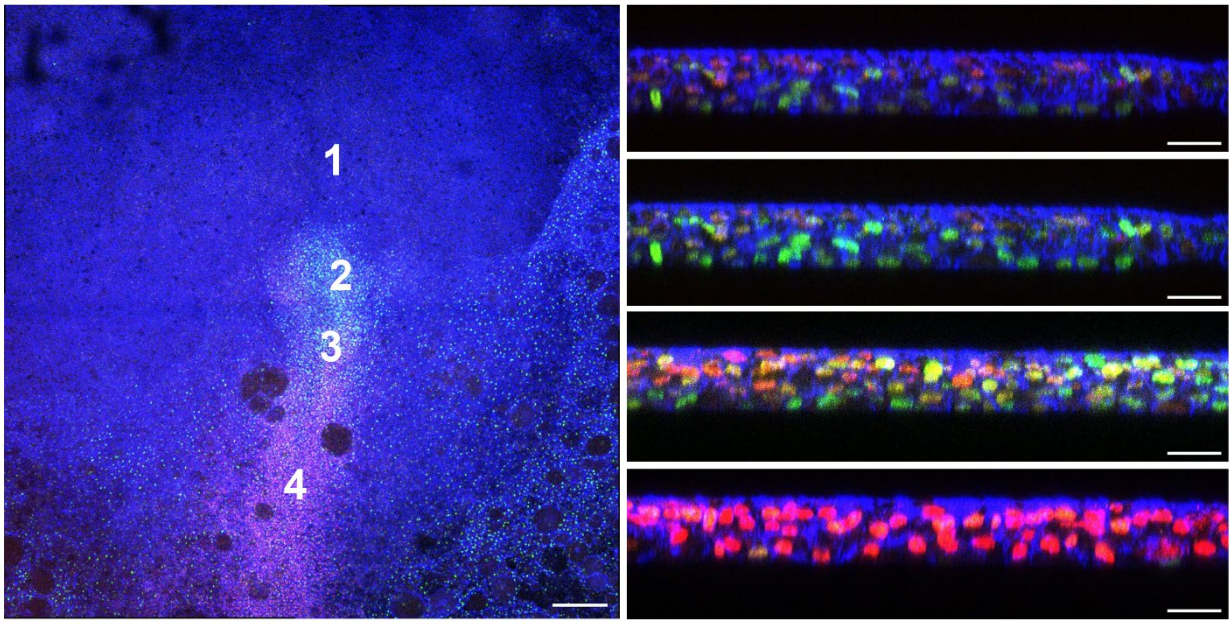

Fig. S11 Comparison of SNAI2 and HNF3B expression in various regions along the streak. (**A**), Image of streak region of HH3 embryo stained for SNAI2 (red), HNF3B (green), and actin (blue). (**B, C,D,E**), sections were taken at positions 1, 2, 3, and 4 indicated in (A).

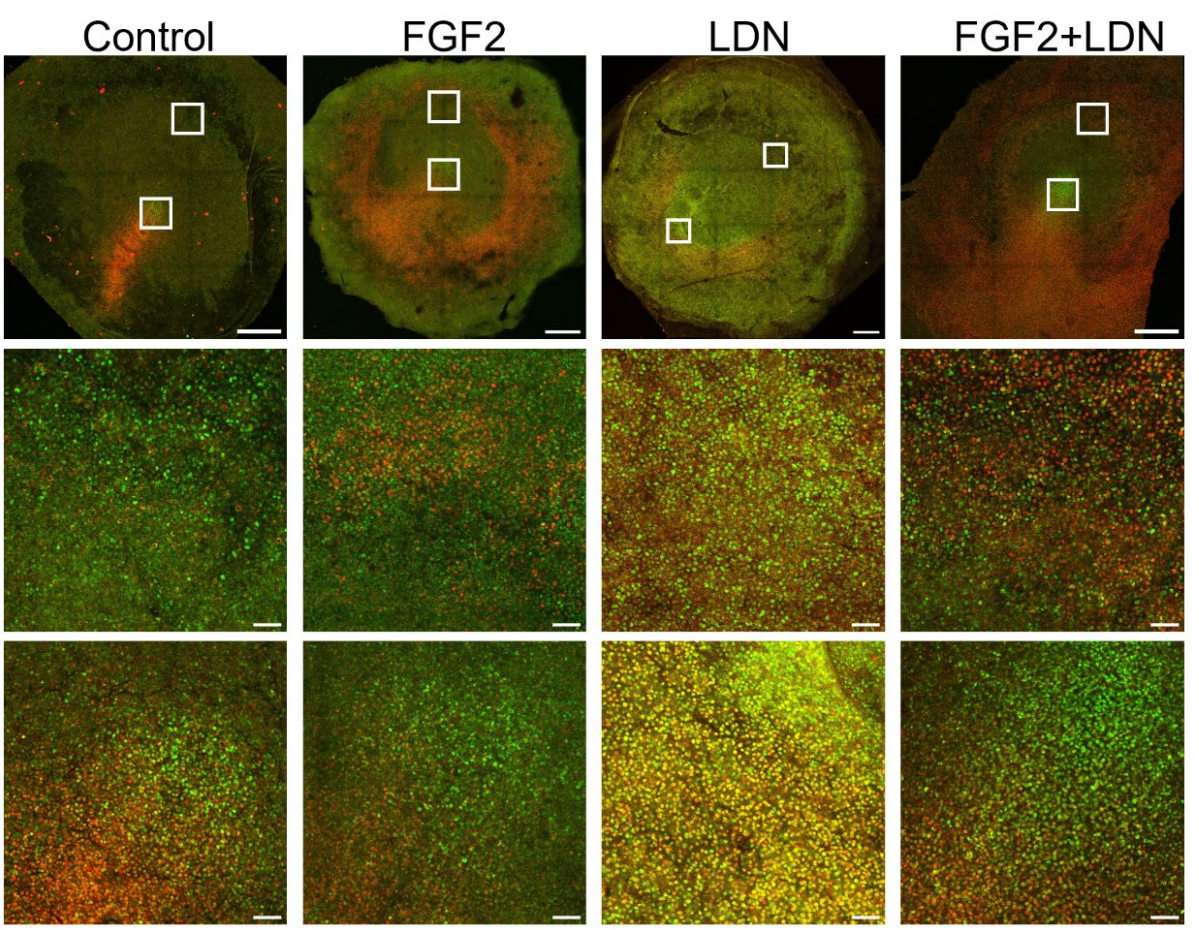

Fig. S12 Comparison of SNAI2 and HNF3B expression after various perturbations. Top row: Brightfield images of embryos after 16hrs in EC culture after various treatments. Second row: Confocal images of the embryos in the top row showing expression of SNAI2 (red) and HNF3B (green). The third and fourth rows show higher magnification images taken in front of the streak (upper white square in each image) and (lower white square in each image) at the tip of the streak. It can be seen in the control (first row) that cells in the tip of the streak are characterized by low expression of SNAI2 and high expression of HNF3B while anterior to the streak few cells express SNAI2, but some scattered cells express HNF3B. FGF treatment results in cells that express SNAI2 in a ring-shaped region at the boundary of the embryonic and extraembryonic area, mixed with cells expressing HNF3B while there is little co-expression. LDN treatment results in a decrease in the expression of SNAI2 and an increase in the expression of HNF3B in the entire epiblast, with many cells co-expressing both factors. Combined treatment of LDN and FGF results in an FGF-like phenotype with increased expression of SNAI2 and less effect on HNF3B expression. Overall, these results may indicate that FGF treatment shifts the differentiation of the cells more towards mesoderm, while LDN treatment may shift the differentiation of the cells more towards endoderm precursors. Scale bars in two top rows of images are 500 μm, and scale bars in two bottom rows of images are 50 μm.

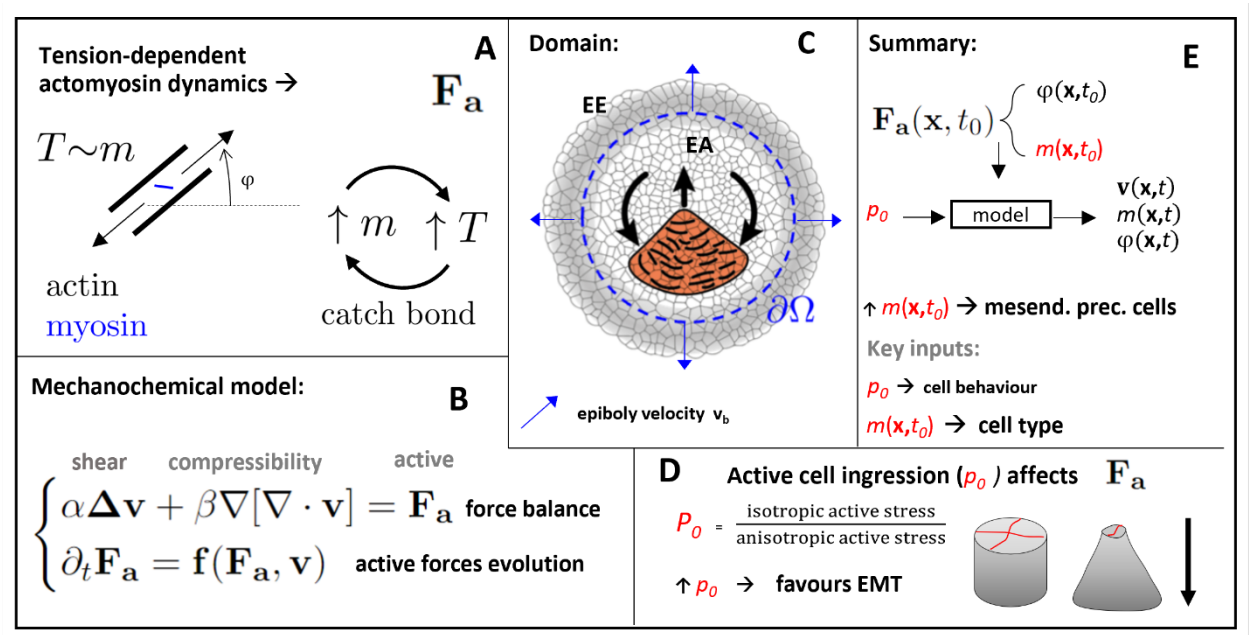

Fig. S13. **Mechanochemical model. (A),** Actomyosin cables generate active forces $\mathbf{F_a}$. $\mathbf{F_a}$ arises from spatial variation of phosphorylated myosin m and the orientation of the actomyosin cables φ. The myosin dissociation rate is tension dependent reflecting the catch-bond mechanism: cables with more myosin accumulate more myosin generating an instability that drives the flow. The φ dynamics is also coupled to the flow velocity $\boldsymbol{v}$, which transports and rotates the actomyosin cables. **(B),** The mechanochemical model consists of a force balance that includes shear forces capturing anisotropic tissue-level deformations and cell intercalations, forces induced by compressibility effects such as cell divisions, ingression and growth, and active forces $\mathbf{F_a}$. The time evolution $\mathbf{F_a}$ is coupled to the flow velocity, as summarized in A. **(C),** The domain's boundary consists of a circular boundary in the Extra-Embryonic (EE) region right outside the Embryonic Area (EA). The radial outward epiboly cell motion in the EE region enters our model as the velocity boundary condition. $\mathbf{v_b}$. **(D),** The active cell ingression (p_0) is a key nondimensional parameter in the model. p_0 is the ratio of isotropic active stress (produced by apical contraction and cell ingression) to anisotropic active stress (oriented cell intercalation). High p_0 models the ability of cells to contract isotopically, actively pulling their neighbors and inducing ingression and EMT. **(E),** Our model requires only the initial condition of $\mathbf{F_a}$, which consists of specifying $\varphi(\mathbf{x}, t_0)$ and $m(\mathbf{x}, t_0)$, and a few constant nondimensional parameters. It then provides the full spatiotemporal evolution of cell velocity, actomyosin cable orientation, and active myosin at later times. In all our model experiments, we change only two key inputs: p_0, $m(\mathbf{x},t_0)$. Decreasing p_0 models the cells' inability to undergo EMT or active cell ingression. Changes in $m(\mathbf{x},t_0)$ modulate the initial distribution of active myosin. We find that regions of high $m(\mathbf{x},t_0)$ are a good proxy for mesendoderm precursor cell type. For more details see (18).

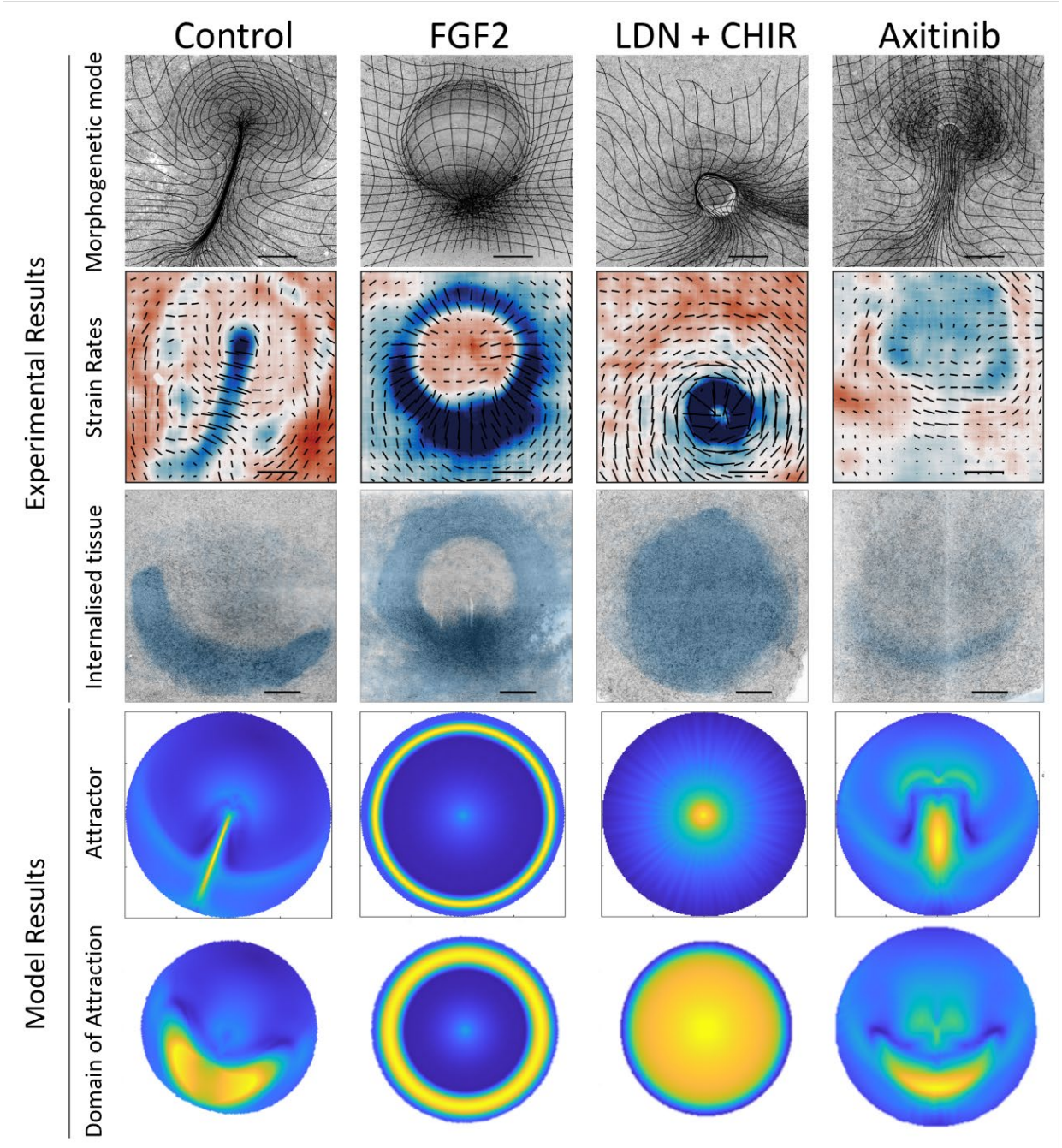

Fig. S14. Comparison of tissue dynamics measure experimentally (rows 1-3) and calculated from the mechano-chemical model (rows 4-5) after different perturbations. First row: Tissue deformation calculated from the tissue velocity field 16hrs after different perturbations as indicated in the legend. Second row: isotropic and anisotropic strain rates. Third row: domain of attraction calculated for experiments, yellow denotes the attractor. Fourth row: Lagrangian attractors. Fifth row: domain of attraction, yellow indicates tissue that will ingress during the experiment. For details of the model see (18). Data in rows 1, 2, and 3 are repetitions of data shown in Fig. 1 and Fig. 2.

Supplementary movies

Movie S1. Development of control embryo from stage HH1 to HH3+. The movie shows the development of a control embryo (left panel) and a zoom-in of the formation of the primitive streak (right panel). Inset side 650 μm. The time interval is 3 minutes.

Movie S2. Strain rates and deformation grid of control embryo from stage HH1 to HH3+. The movie shows a bright field image (top panel) and strain rate tensor of the same embryo (bottom panel) Isotropic strain rate is colored blue (contraction) to red (expansion) scale bar 500 μm. The time interval is 3 minutes.

Movie S3. Development of embryo treated with FGF signaling inhibitor LY287455. The movie shows a bright field image (top panel) and strain rate tensor of the same embryo (bottom panel). Isotropic strain rate is colored blue (contraction) to red (expansion) scale bar 500 μm. The time interval is 3 minutes.

Movie S4. Formation of an ectopic circular primitive streak in FGF2 treated embryo. The movie shows the development of an FGF2-treated embryo (left panel) and a zoom-in of the formation of the ectopic circular primitive streak (right panel). Inset side 650 μm. The time interval is 3 minutes.

Movie S5. Strain rates and deformation grid of embryo treated with FGF2. The movie shows a bright field image (top panel) and strain rate tensor of the same embryo (bottom panel) Isotropic strain rate colored blue (contraction) to red (expansion) scale bar 500 μm. The time interval is 3 minutes.

Movie S6. Migration of mesoderm cells after addition of FGF2. Focusing deeper into the embryo shows that the mesoderm cells ingressing through the circular primitive streak migrate towards the center of the embryo. The time interval is 3 minutes.

Movie S7. Formation of large invagination of the central epiblast in embryos treated with CHIR+LDN. The movie shows the development of a CHIR + LDN treated embryo (left panel) and a zoom-in of the formation of the large invagination in the central epiblast (right panel). Inset side 650 μm. The time interval is 3 minutes.

Movie S8. Strain rates and deformation grid of embryo treated with CHIR+LDN. The movie shows a bright field image (top panel) and strain rate tensor of the same embryo (bottom panel) Isotropic strain rate colored blue (contraction) to red (expansion) scale bar 500 μm. The time interval is 3 minutes.

Movie S9. Formation of an invaginating lip in an embryo treated with Axitinib. The movie shows the development of an Axitinib-treated embryo (left panel) and a zoom-in of the formation of the invaginating lip (right panel). Inset side 650 μm. The time interval is 3 minutes.

Movie S10. Strain rates and deformation grid of embryo treated with Axitinib. The movie shows a bright field image (left panel) and strain rate tensor of the same embryo (right panel) Isotropic strain rate colored blue (contraction) to red (expansion) scale bar 500 μm. The time interval is 3 minutes.

Movie S11. Comparison of the tip of streak formation in control embryo and embryo treated with 100 nM Axitinib. The time interval is 3 minutes.